

Shallow Enclosure Horizontal Convection: Insights from Asymptotic Expansion Analysis

Sajjad Hossain, Tony Vo and Gregory J. Sheard

Department of Mechanical & Aerospace Engineering
 Monash University, Victoria 3800, Australia

Abstract

Horizontal convection is a distinctive convection heat transfer process where heating and cooling occurs along the same horizontal boundary. This study employs the asymptotic expansion method to elucidate Nusselt and Rayleigh number relationships toward the limits of small aspect ratios. Expansion solutions are derived and compared with the high-order spectral element simulations obtained for a rectangular enclosure of length L , height, H (aspect ratio, $A = H/L$), at a Prandtl number of $Pr = 6.14$ (consistent with water) across a wide span of Rayleigh numbers, ($10 \leq Ra \leq 10^{16}$) and aspect ratios ($10^{-3} \leq A \leq 0.16$). The Boussinesq flow is driven by imposing a linear temperature variation from colder to warmer across the bottom boundary of the enclosure, and insulating temperature conditions on the remaining boundaries. The accuracy of the model is demonstrated by comparison with the numerical solutions, and second-order expansion solutions captured the Nusselt-Rayleigh number behaviour.

Keywords

Horizontal convection; shallow enclosure; heat transfer; asymptotic expansion.

Introduction

Horizontal convection is classified as a distinctive version of natural convection, where heating and cooling occurs exclusively along the horizontal boundary of the enclosure. In contrast to the substantially studied Rayleigh–Bénard convection, where convective overturning circulation is stimulated by both heating and cooling, the strength of overturning circulation in horizontal convection is dominated by heat diffusion [1]. Research on horizontal convection has been inspired by the transport of warm fluids in the oceanic circulation and engineering processes, like glass melting in furnaces [2].

Several experimental and numerical studies on horizontal convection investigated the flow dynamics and heat transfer scaling. Experiments by Mullarney et al. [3] with water in an enclosure of aspect ratio (height to length), $A=0.16$ showed that beyond the diffusion-dominated regime, the Nusselt number (Nu) scales approximately with $Ra^{1/5}$, which is similar to the Rossby scaling [4]. Sheard and King [5] used a spectral element method to investigate horizontal convection for aspect ratios, $0.16 \leq A \leq 2.0$ at a range of Rayleigh and fixed Prandtl number representative of water ($Pr = 6.14$). They reported an aspect ratio dependence based on the measured Nu and boundary layer thickness at low Ra . The authors also confirmed an increase in the exponent of Ra $1/5^{\text{th}}$ to $1/3^{\text{rd}}$ in the convective regime for

the Nu scaling. This uplift was later shown to represent a shift between flow regimes both obeying $Nu \propto Ra^{1/5}$ [6].

Despite the substantial motivation to study horizontal convection to reveal the role of buoyancy forcing in ocean currents, the previous widely studied range of enclosure aspect ratios ($A \geq 0.16$) is at least two orders of magnitude larger compared to the ocean-relevant values ($10^{-5} \leq O(A) \leq 10^{-3}$). Therefore, certain aspects the shallow enclosure horizontal convection remains unexplored. This study emphasises on providing insights into Nusselt-Rayleigh number relationships of horizontal convection employing an asymptotic expansion analysis and exploring the theoretical shape of the Nusselt number which characterises the onset of the non-linear effects in shallow enclosure horizontal convection flow.

Model derivation

The computation domain comprises a rectangular enclosure, having internal dimensions of length L , height, H (aspect ratio, $A = H/L$) as shown in figure 1. The flow is driven by a linear temperature profile applied along the bottom boundary of the enclosure. The side and top walls are thermally insulated (a zero wall-normal temperature gradient is imposed), and a no-slip condition is imposed on the velocity field on all walls. The buoyancy is modelled with the Boussinesq approximation, in

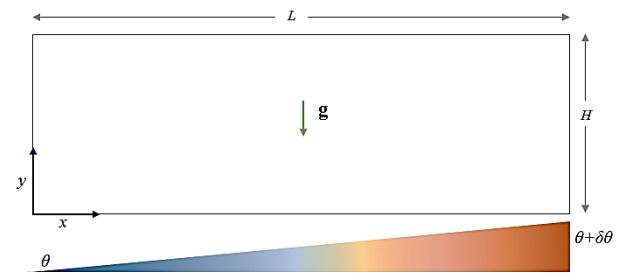


Figure 1. A schematic diagram of the system. The origin of the coordinate system placed at the bottom-left corner, and a temperature difference of $\delta\theta$ imposed along the bottom boundary.

which density differences in the fluid are disregarded except for the contribution of gravity. The Navier–Stokes equations governing a Boussinesq fluid are written as

$$\nabla \cdot \mathbf{u} = 0, \quad (1a)$$

$$\frac{\partial \mathbf{u}}{\partial t} + (\mathbf{u} \cdot \nabla) \mathbf{u} = -\frac{1}{\rho_0} \nabla p^* + \nu \nabla^2 \mathbf{u} + \alpha g e_y (\theta - \theta_0) \quad (1b)$$

$$\frac{\partial \theta}{\partial t} = -(\mathbf{u} \cdot \nabla) \theta + \kappa \nabla^2 \theta, \quad (1c)$$

where t is time, θ is the temperature, p^* is the pressure with hydrostatic contribution, \mathbf{u} denotes the velocity vector, \mathbf{g}_y is a unit vector in the direction of gravity, ρ_o is defined as the reference density of the fluid and κ is the thermal diffusivity. To introduce non-dimensionalisations (primes denote the described dimensionless quantities) we define

$$\mathbf{x} = L(x', y'), \quad t = \frac{L^2}{\kappa} t', \quad \mathbf{u} = \frac{\kappa}{L} (u', v'), \quad p^* = \rho_o \frac{\kappa^2}{L^2} p'^*,$$

$$\nabla = \frac{1}{L} \left(\frac{\partial}{\partial x'}, \frac{\partial}{\partial y'} \right), \quad \nabla^2 = \frac{1}{L^2} \left(\frac{\partial^2}{\partial x'^2} + \frac{\partial^2}{\partial y'^2} \right), \quad \theta = \theta_0 + \partial \theta \theta'.$$

Length, time, velocity, pressure and temperature difference are respectively scaled by L , L^2/κ , κ/L , $\rho_o \kappa^2/L^2$ and $\partial \theta$. The non-dimensionalised form (excluding the primes for convenience) of equations (1a) to (1c) and splitting momentum into its horizontal and vertical parts leaves

$$\frac{\partial u}{\partial x} + \frac{\partial v}{\partial y} = 0, \quad (2a)$$

$$\frac{\partial u}{\partial t} + u \frac{\partial u}{\partial x} + v \frac{\partial u}{\partial y} = -\frac{\partial p}{\partial x} + Pr \left(\frac{\partial^2 u}{\partial x^2} + \frac{\partial^2 u}{\partial y^2} \right), \quad (2b)$$

$$\frac{\partial v}{\partial t} + u \frac{\partial v}{\partial x} + v \frac{\partial v}{\partial y} = -\frac{\partial p}{\partial y} + Pr \left(\frac{\partial^2 v}{\partial x^2} + \frac{\partial^2 v}{\partial y^2} \right) + Pr Ra \theta, \quad (2c)$$

$$\frac{\partial \theta}{\partial t} + u \frac{\partial \theta}{\partial x} + v \frac{\partial \theta}{\partial y} = \frac{\partial^2 \theta}{\partial x^2} + \frac{\partial^2 \theta}{\partial y^2}. \quad (2d)$$

Here we have introduced the Prandtl number, $Pr = \nu/\kappa$ and Rayleigh number $Ra = \alpha g \partial \theta L^3 / \nu \kappa$. Now, expanding the variables in terms of Ra ,

$$\chi = Ra^0 \chi_0 + Ra^1 \chi_1 + Ra^2 \chi_2 + \dots \quad (3)$$

where $\chi = u, p$ and θ . Substituting (3) into the equations (2a) to (2d) and collecting terms of zero order yields

$$\frac{\partial u_0}{\partial x} + \frac{\partial v_0}{\partial y} = 0, \quad (4a)$$

$$\frac{\partial u_0}{\partial t} + u_0 \frac{\partial u_0}{\partial x} + v_0 \frac{\partial u_0}{\partial y} = -\frac{\partial p_0}{\partial x} + Pr \left(\frac{\partial^2 u_0}{\partial x^2} + \frac{\partial^2 u_0}{\partial y^2} \right), \quad (4b)$$

$$\frac{\partial v_0}{\partial t} + u_0 \frac{\partial v_0}{\partial x} + v_0 \frac{\partial v_0}{\partial y} = -\frac{\partial p_0}{\partial y} + Pr \left(\frac{\partial^2 v_0}{\partial x^2} + \frac{\partial^2 v_0}{\partial y^2} \right), \quad (4c)$$

$$\frac{\partial \theta_0}{\partial t} + u_0 \frac{\partial \theta_0}{\partial x} + v_0 \frac{\partial \theta_0}{\partial y} = \frac{\partial^2 \theta_0}{\partial x^2} + \frac{\partial^2 \theta_0}{\partial y^2}. \quad (4d)$$

As the enclosure has no-slip boundary conditions on all boundaries and the zeroth order equations have eliminated buoyancy there is no mechanism in these equations to drive the flow. In addition, the velocity field is no longer a function of the temperature field. Considering the equilibrium state, it is apparent that the velocity field must approach zero at long times. With a zero-velocity field and assuming a steady state, equations (4a) – (4d) reduce to

$$u_0 = v_0 = \frac{\partial p_0}{\partial x} = \frac{\partial p_0}{\partial y} = 0, \quad (5a)$$

$$\frac{\partial^2 \theta_0}{\partial x^2} + \frac{\partial^2 \theta_0}{\partial y^2} = 0. \quad (5b)$$

Thus, zeroth order solution comprises a zero-velocity field, an arbitrary constant pressure field, and a temperature field obtained by conduction through the stationary fluid satisfying

the imposed-temperature and insulating boundary conditions. Now attention is turned to collect the first-order terms considering values from (5a) and (5b),

$$\frac{\partial u_1}{\partial x} + \frac{\partial v_1}{\partial y} = 0, \quad (6a)$$

$$\frac{\partial p_1}{\partial x} = Pr \left(\frac{\partial^2 u_1}{\partial x^2} + \frac{\partial^2 u_1}{\partial y^2} \right), \quad (6b)$$

$$\frac{\partial p_1}{\partial y} = Pr \left(\frac{\partial^2 v_1}{\partial x^2} + \frac{\partial^2 v_1}{\partial y^2} \right) + Pr \theta_0, \quad (6c)$$

$$u_1 \frac{\partial \theta_0}{\partial x} + v_1 \frac{\partial \theta_0}{\partial y} = \frac{\partial^2 \theta_1}{\partial x^2} + \frac{\partial^2 \theta_1}{\partial y^2}. \quad (6d)$$

From equations (6a) – (6d) we observe that continuity is satisfied, and a balance between first-order pressure and velocity diffusion exists, with a non-zero first-order flow driven by the zeroth-order temperature field. A first-order thermal field arises from a Poisson equation with RHS constructed from the zeroth-order temperature and first-order velocity field. Passing the information obtained from the zeroth and first order equations to deduce the second-order terms

$$\frac{\partial u_2}{\partial x} + \frac{\partial v_2}{\partial y} = 0, \quad (7a)$$

$$\frac{\partial u_2}{\partial t} + u_1 \frac{\partial u_1}{\partial x} + v_1 \frac{\partial u_1}{\partial y} = -\frac{\partial p_2}{\partial x} + Pr \left(\frac{\partial^2 u_2}{\partial x^2} + \frac{\partial^2 u_2}{\partial y^2} \right), \quad (7b)$$

$$\frac{\partial v_2}{\partial t} + u_1 \frac{\partial v_1}{\partial x} + v_1 \frac{\partial v_1}{\partial y} = -\frac{\partial p_2}{\partial y} + Pr \left(\frac{\partial^2 v_2}{\partial x^2} + \frac{\partial^2 v_2}{\partial y^2} \right) + Pr \theta_1, \quad (7c)$$

$$\frac{\partial \theta_2}{\partial t} + u_1 \frac{\partial \theta_1}{\partial x} + u_2 \frac{\partial \theta_0}{\partial x} + v_1 \frac{\partial \theta_1}{\partial y} + v_2 \frac{\partial \theta_0}{\partial y} = \frac{\partial^2 \theta_2}{\partial x^2} + \frac{\partial^2 \theta_2}{\partial y^2}. \quad (7d)$$

In the momentum equations (7b) - (7c), quadratic terms involving products of zeroth and second order velocity fields are omitted as the zeroth order field was zero; likewise, in the thermal transport equation (7d) quadratic terms involving the product of zeroth order velocity and second-order temperature gradients have also been omitted. The second-order velocity field is a function of only first order velocity and temperature fields, and the second-order temperature field is a function of first and second-order velocity, and zeroth and first-order temperature fields. The governing equations are solved by a high-order in-house solver, which employs a spectral-element method for spatial discretisation and a third-order time integration scheme based on backwards-differencing. Meshes are constructed for various aspect ratios from $A = 0.16$ down to 0.001 while setting the most widely studied lowest aspect ratio ($A = 0.16$) in the literature as the largest for the aspect ratio range used in the current study.

Simulation results

Three aspect ratios ($A=0.08, 0.04$ and 0.01) were chosen to calculate different-order Nu by employing the expansion series solutions. Figure 2 illustrates zeroth (Nu_{order0}), first (Nu_{order1}) and second order (Nu_{order2}) Nusselt number for three aspect ratios along with their respective baseflow solutions ($Nu_{baseflow}$) for a range of Ra . The Ra which marks the departure of $Nu_{baseflow}$ from the Nu_{order0} solution demonstrates the onset of the first and second order effects in the flow. This Ra will be termed as Ra_d , and signifies the entrance of the higher-order and non-linear effects of the flow. As the aspect ratio gets smaller, we can see from figure 2 (b) and 2 (c) that Ra_d shifts to higher Ra . The high Ra_d reveals a delayed onset of the higher-order effects owing to the vertical confinement of the enclosures as it gets shallower.

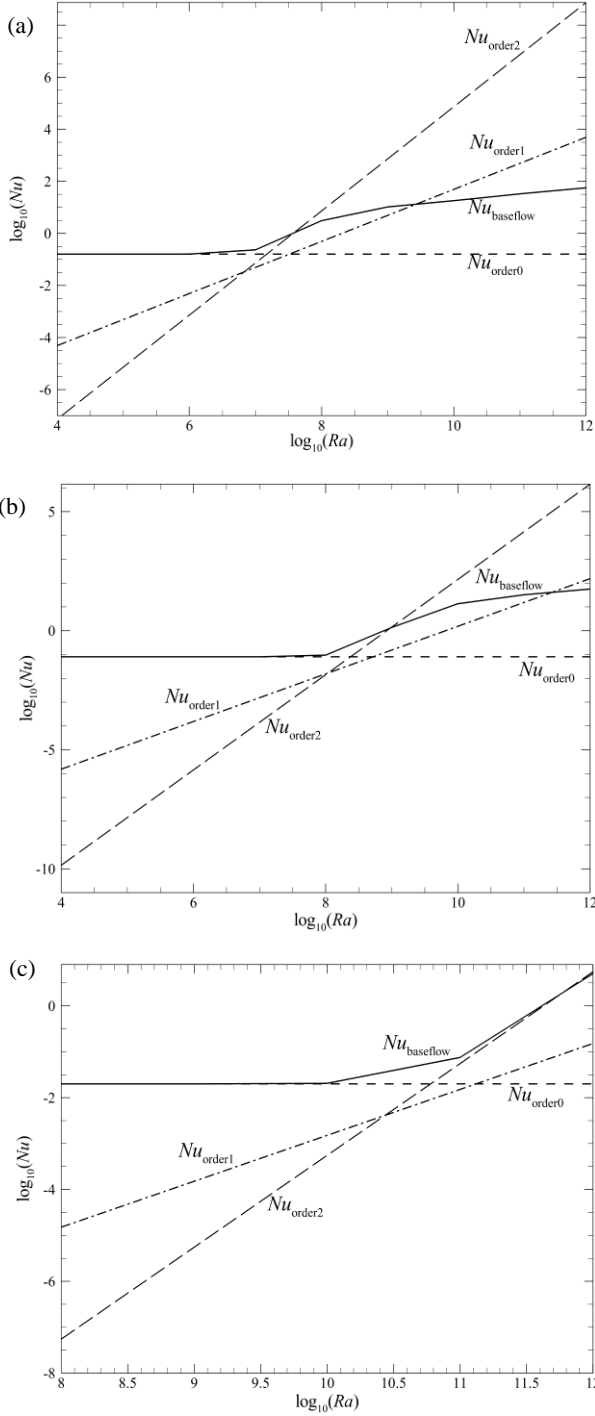


Figure 2. Nu against Ra for different order expansion solution for (a) $A=0.08$, (b) $A=0.04$ and (c) $A=0.01$.

Attention is now turned towards the cumulative Nusselt numbers of the aspect ratios. First-order cumulative Nusselt number ($Nu_{order01}$) sums up the contribution from zeroth and first order terms. Second-order cumulative Nusselt number ($Nu_{order012}$) has the $Nu_{order01}$ and Nu_{order2} terms. Figure 3 depicts the cumulative Nusselt numbers for three different aspect ratios with their respective baseflow solutions. As the cumulative Nusselt numbers sum up from the zeroth to any respective order terms, it elucidates the impact of that specific (first or second) order term, which is described in Figure 2. Figure 3 (a) illustrates that the cumulative Nusselt numbers for $A=0.08$ demonstrate $Nu_{order012}$ can capture the baseflow solution features to a higher Ra than $Nu_{order01}$. For smaller aspect ratios, the $Nu_{order012}$ gets much closer to the baseflow solutions

compared to $Nu_{order01}$. It can be seen from figure 3 (b) and (c) that the $Nu_{order012}$ term progressively coincides more with the baseflow for $A=0.04$ and $A=0.01$ compared to the larger aspect ratio ($A=0.08$). For $A=0.01$, the $Nu_{order012}$ term captures the baseflow solution up to $\log_{10}(Ra) \approx 11.5$.

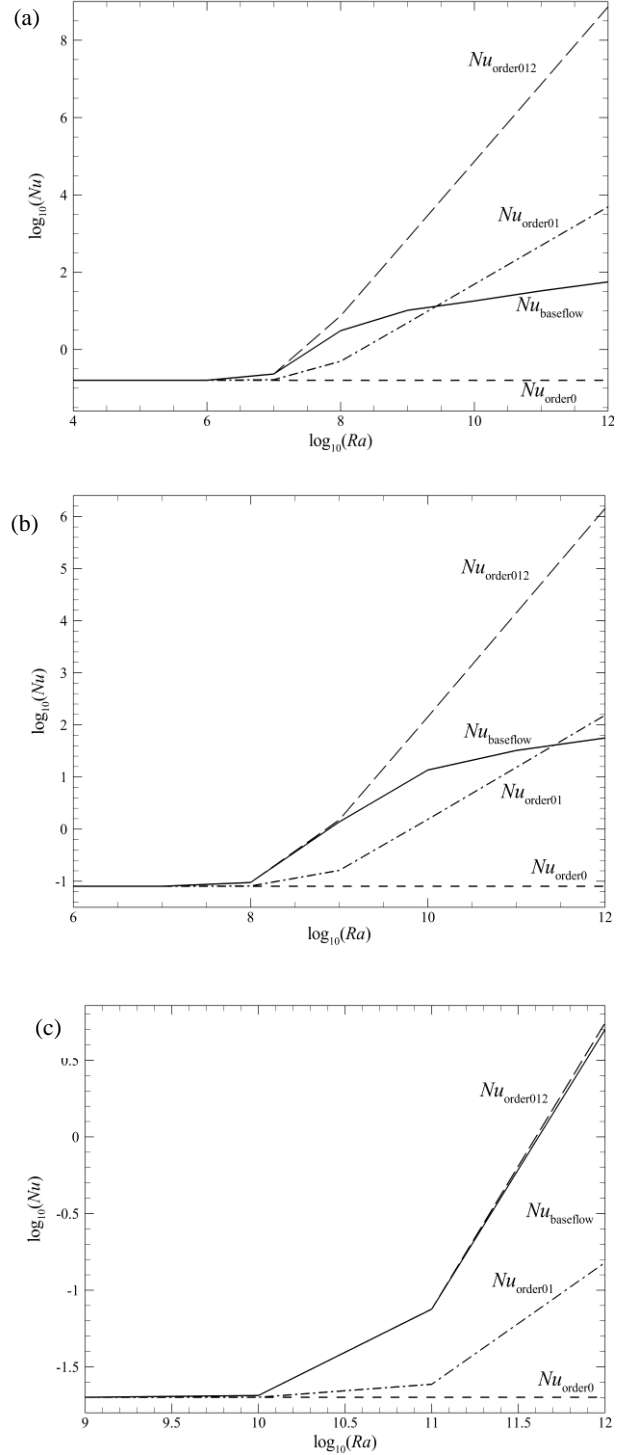


Figure 3. Cumulative Nu against Ra for different order expansion solution for (a) $A=0.08$, (b) $A=0.04$ and (c) $A=0.01$.

Previous published work [7] from the authors' explored different regimes and revealed the relationships of Nusselt number, Rayleigh number and aspect ratios. Based on the low- Ra /low- A scaling of $Nu \sim A$ and $Ra \sim A^{-4}$, the $Nu - Ra$ data is plotted in figure 4. For lower values of RaA^4 , the corresponding values of Nu/A can be seen to have collapsed onto a universal

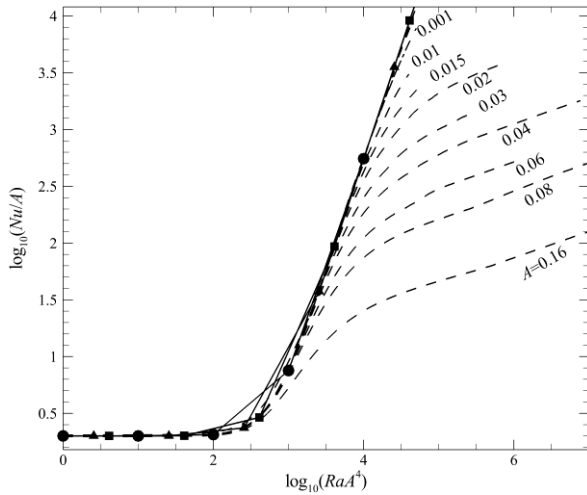


Figure 4. Scaled Nu - Ra plots with dashed lines features a range of aspect ratios ($10^{-3} \leq A \leq 0.16$) with the expansion solutions of three aspect ratios. For $A = 0.08, 0.04$ and 0.01 , expansion solutions are scaled and plotted using a solid line with square, triangle, circle symbols, respectively.

curve for all aspect ratios. After $\log_{10}(RaA^4) \approx 1.75$ the Nu/A values for all aspect ratios start branching off for $\log_{10}(RaA^4) \geq 1.75$, starting with the highest $A = 0.16$ and then in descending order to the lowest $A = 0.001$ with increasing Rayleigh number. This branching off resembles the convection-dominated regime of the shallow enclosure horizontal convection. To validate the expansion series results, the cumulative second order Nusselt numbers for $A = 0.08, 0.04$ and 0.01 are scaled and included in figure 4. We can see that the expansion series solutions follow the universal collapse trend until the convection-dominated region.

Conclusion

This study entails asymptotic expansion series to elucidate the Nusselt-Rayleigh number behaviour in shallow enclosure horizontal convection and provide insight regarding the onset of the non-linear behaviour of the flow. Zeroth, first and second order expansion solutions are derived from the governing equations. A Rayleigh number, Ra_d that predicts the onset of the higher order and non-linear effects is introduced based on the departure of the different order Nusselt numbers from the baseflow solution. An increase in Ra_d is observed as the aspect ratio gets smaller. Expansion series solutions are also validated

against the scaled Nusselt-Rayleigh number plot consisting of thirteen aspect ratios. The scaled Nusselt number changes with squared value of scaled Rayleigh number, $Nu/A \sim (RaA^4)^2$. The cumulative second order Nusselt number from the expansion solution demonstrates a collapse along with the universal trend of the scaled Nusselt number. It reveals that the second order expansion solutions manifest the quadratic Nusselt-Rayleigh behaviour until the commencement of convection-dominated regime of the shallow enclosure horizontal convection.

Acknowledgments

This research work was supported by the Australian Research Council through Discovery Grants DP150102920 and DP180102647 and was undertaken using the peak high-performance computing facility of the National Computational Infrastructure (NCI) thanks to a grant under the National Computational Merit Allocation Scheme (NCMAS).

References

- [1] Hughes, G.O. and R.W. Griffiths, *Horizontal convection*. Annu. Rev. Fluid Mech., 2008. 40: p. 185-208.
- [2] Paparella, F., *Turbulence, Horizontal Convection, and the Ocean's Meridional Overturning Circulation*, in Mathematical Paradigms of Climate Science. 2016, Springer. p. 15-32.
- [3] Mullarney, J.C., R.W. Griffiths, and G.O. Hughes, *Convection driven by differential heating at a horizontal boundary*. Journal of Fluid Mechanics, 2004. 516: p. 181-209.
- [4] Rossby, H. *On thermal convection driven by non-uniform heating from below: an experimental study*. in Deep Sea Research and Oceanographic Abstracts. 1965. Elsevier.
- [5] Sheard, G.J. and M.P. King, *Horizontal convection: effect of aspect ratio on Rayleigh number scaling and stability*. Applied Mathematical Modelling, 2011. 35(4): p. 1647-1655.
- [6] Gayen, B., R.W. Griffiths, and G.O. Hughes, *Stability transitions and turbulence in horizontal convection*. Journal of Fluid Mechanics, 2014. 751: p. 698-7.
- [7] Hossain, S., T. Vo, and G.J. Sheard, *Horizontal convection in shallow enclosures scales with height, not length, at low Rayleigh numbers*. International Communications in Heat and Mass Transfer, 2019. 109: p. 1043